References

Claerbout, J. F., 1976, Fundamentals of Geophysical Data Processing, McGraw-Hill, New York.

--- 1970, Coarse grid calculations of waves in inhomogeneous media with application to delineation of complicated seismic structure: Geophysics, v. 35, no. 3, p. 407-418.

--- 1971, Toward a unified theory of reflector mapping: Geophysics, v. 36, no. 3, p. 467-481.

Claerbout, J. F. and A. G. Johnson, 1971, Extrapolation of time dependent waveforms along their path of propagation: Geophys. Journ. of the Roy. Astr. Soc., v. 26, no. 1-4, p. 285-294.

Claerbout, J. F. and S. M. Doherty, 1972, Downward continuation of moveout corrected seismograms: Geophysics, v. 37, no. 5, p. 741-768.

Dix, C. H., 1955, Seismic velocities from surface measurements: Geophysics, v. 20, p. 68-86.

Doherty, S. M., 1975, Structure independent seismic velocity estimation, Ph.D. thesis, Stanford University.

Doherty, S. M., and J. F. Claerbout, 1976, Structure independent seismic velocity estimation, Geophysics, in press.

Levin, F. K., 1971, Apparent velocity from dipping interface reflections: Geophysics, v. 36, no. 3, p. 510-516.

Peterson, R. A., and W. C. Walter, 1974, Through the kaleidoscope, a doodlebugger in Wonderland: United Geophysical Corporation publication.

Riley, D. C., 1975, Wave equation synthesis and inversion of diffracted multiple seismic reflections, Ph.D. thesis, Stanford University.

Riley, D. C., and J. F. Claerbout, 1976, 2-D Multiple Reflections, Geophysics, v. 38, no. 5, p. 592-620.

Slotnick, N. M., 1959, Lessons in seismic computing: Tulsa, Society of Exploration Geophysicists.

Stacey, F. D., 1969, Physics of the earth: John Wiley and Sons, New York.

Appendix A

End Effects and Aliasing

In our discussions of slant wave stacked data, we had implicitly assumed that a stack over any desired ray parameter, $p = \frac{\sin\theta}{v}$, could be done, with the resultant data display precisely that which we would have obtained from a downgoing conical wave propagating at some angle, θ, to the vertical. This for the most part remains true, but only with respect to two important practical considerations: our data (in the form of common shot or common geophone gathers) are 1) of finite spatial and temporal extent, and 2) discretely sampled in space and time. The first item imposes on us the problem of end effects, while the second can introduce aliasing.

The manner in which the truncation of the data can produce end effects is shown in Figure A1. The only contribution to a slant sum should be from the region of tangency, but a small contribution will arise from the termination of the data at the near and far offsets. These end effects have been noticed by us in our previous attempts to slant stack field data. The far trace end effect (the dotted line in Figure A1) can be easily seen in the slant stacks in the previous section. They appear as a "ghosting" of the sea floor at $t \tilde{>} 2$ seconds. The near trace end effect (the dashed line in Figure A1) cannot as readily be identified in these stacks, but must certainly be present at closer proximity to the primary energy.

There must certainly be many approaches that will be effective in reducing end effects, but the one that we shall use has the advantage of being computationally cheap.

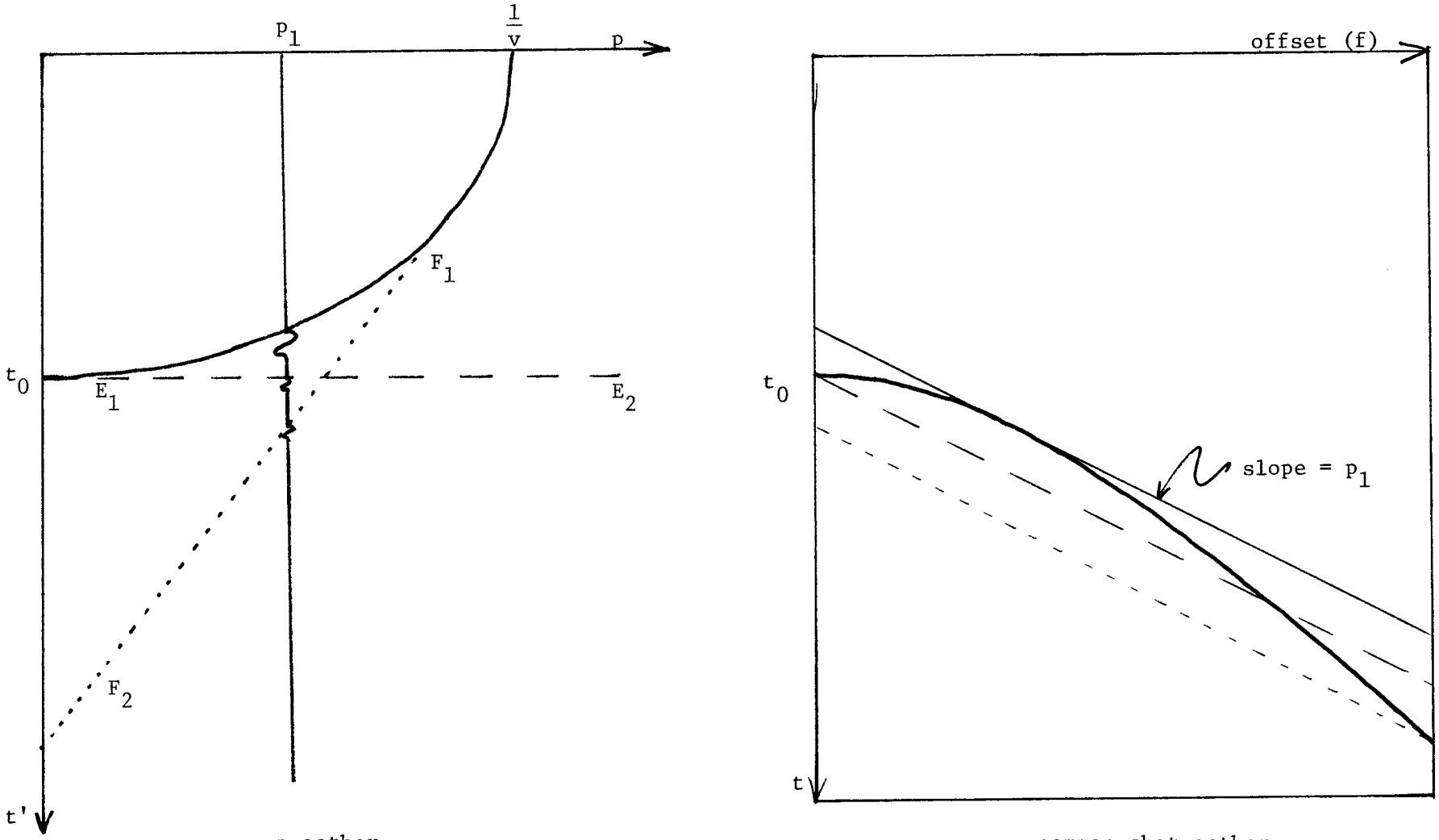

p-gather

common shot gather

Figure A1. The end effect problem. The frame to the right shows a common shot (or geophone) gather with a single hyperbolic event portrayed. If we do a slant stack over ray parameter $p = p_1$, we get the main contribution in the stationary phase summation at the point of tangency, shown as the sloping line. The two

(continued on following page)

Fig. A1 (Cont'd.).

other sloping lines, the dashed and the dotted lines, show non-zero contributions to the summation due to the near (line E_1E_2) and far (line F_1F_2) offset truncations of the data.

The frame to the left shows the p-gather produced from the common shot gather. The portion of an ellipse drawn as a solid line is the main event. Its intercepts are at $t = t_0$ and $p = 1/v$. The dashed and dotted lines show where the two end effects map into this domain. The trace at $p = p_1$ is drawn.

Figure A2 shows how we can sample past the end traces if we have some knowledge of velocity. Sampling n traces off the end of the cable can be equivalenced to resampling and summing a region δt, of the last trace. But rather than sampling the last trace so coarsely (shown by the small circles in Figure A2, we can instead use all time points in the region δt to insure against possible aliasing.

Observing Figure A2 we can write immediately

$$\left[\left(\frac{dt}{df}\right)_e - \left(\frac{dt}{df}\right)_s \right] n \Delta f = \delta t \qquad (A1)$$

where f is the offset coordinate, subscript "e" refers to the trajectory of the event, subscript "s" refers to the trajectory of the slant stack summation, Δf is the horizontal sampling interval (geophone spacing), and n is the number of traces off the end of the cable.

Let

$$\delta t = \gamma \Delta t \qquad (A2)$$

where Δt is the sampling interval on the time axis, and γ is some number (not necessarily integral).

From the equation for the event, e,

$$t^2 = t_0^2 + \frac{f^2}{v^2} \qquad (A3)$$

we have

$$\left(\frac{dt}{df}\right)_e = \frac{f}{t\, v^2} \qquad (A4)$$

and trivially,

$$\left(\frac{dt}{df}\right)_s = p \qquad (A5)$$

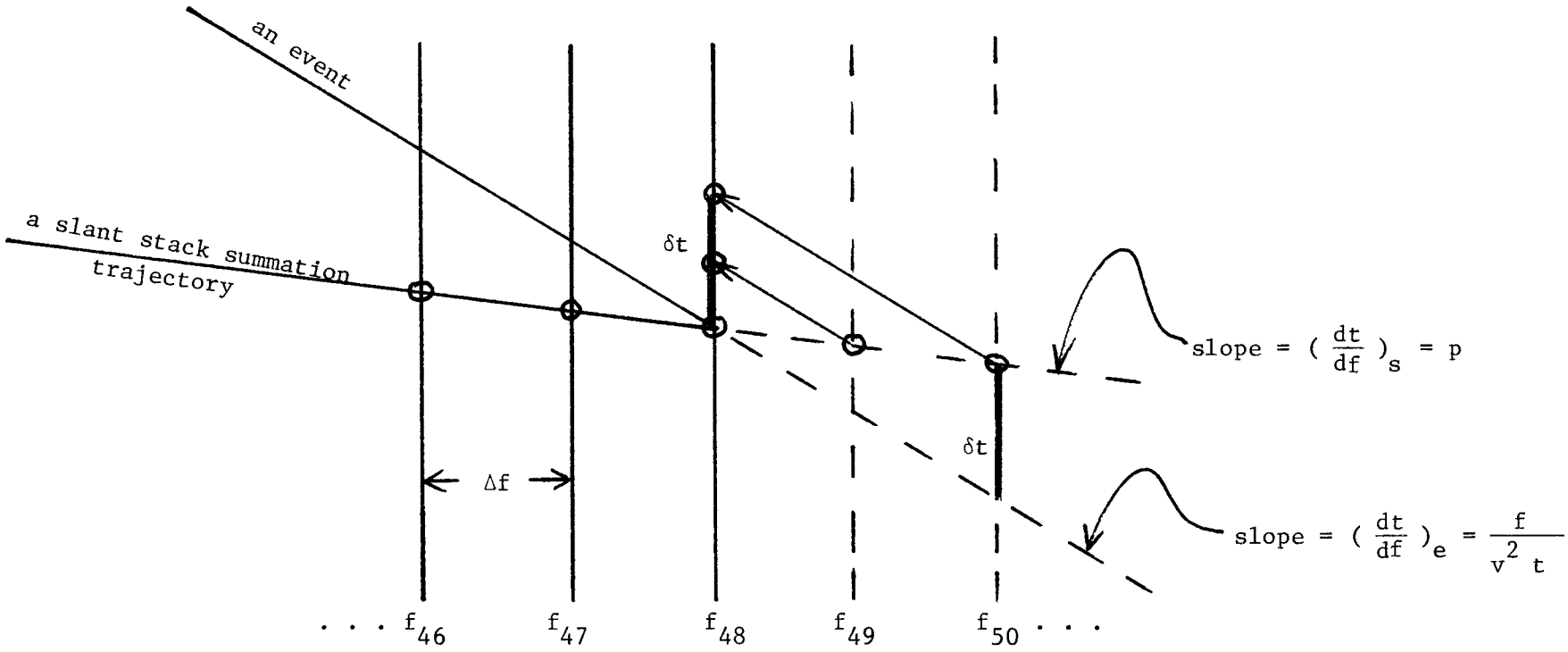

Figure A2. An approach to reducing end effects. The final three traces of a 48-trace common shot (or geophone) gather is shown with two hypothetical traces added. The small circles show where the traces are to be sampled in the summation. With knowledge of velocity, sampling of traces off the end of the cable can be approximated by sampling the last trace in the manner suggested in the figure. Formulas are derived in the text. This trick is also applied to the inner trace.

giving an expression for γ ,

$$\gamma = n\left(\frac{\Delta f}{\Delta t}\right)\left(\frac{f}{t\,v^2} - p\right) \qquad \text{(A6)}$$

The above result tells us how many time points to sum "upward" on the last trace ($f = f_{max}$) or "downward" on the first trace ($f = f_{min}$) to include n traces off the end of the cable into the sum.

Our choice of n must be made moderate because of our uncertainty in v , and because the slope of the event will change between f_{max} and f_{max+n} . We are currently using $n = 6$.

The form of equation (A6) shows that for a stack over a single value of p , the first and last traces in the common shot (geophone) gather can be recomposed by replacing each time point by a sum over the proper interval $\gamma\,\Delta t$, predicted by equation (A6). The slant stack can then procede simply.

Figure A3 shows how aliasing can be introduced into the slant stack. When the slant sum trajectory intercepts an event at a large angle, finite spatial sampling will at some point lead to aliasing.

As with end effects, there are many workable methods to eliminate or reduce this type of aliasing. Our approach is to "window" the data so that we include only those data which we expect will contribute to the slant sum.

Figure A4 shows that the general shape of the anti-aliasing window is a wedge with its apex at the origin. For a given value of p , we now determine the parameters of the window. For the present we assume v is constant and of known value.

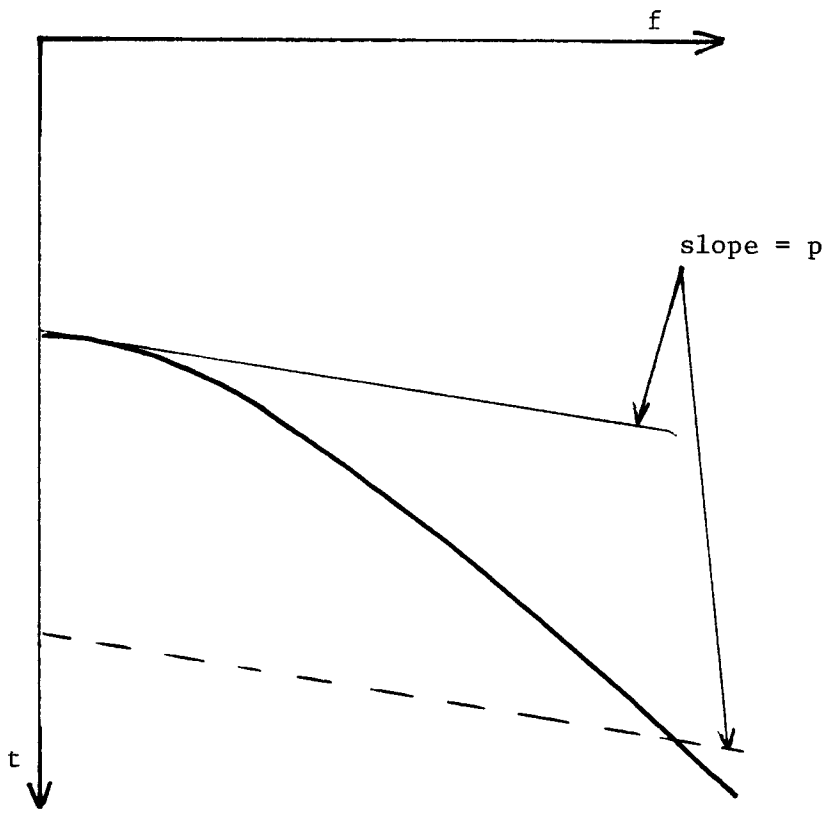

Figure A3. A common geophone gather showing slant summation trajectory for some p. The solid sloping line shows the trajectory for the summation at point of tangency. The dashed line shows another summation trajectory which should add to zero (or whatever small quantity is predicted by the continuous solution). However, since at this point we are summing across the event at a steep angle, the finite sampling interval in the x coordinate can cause aliasing, thereby introducing spurious energy into the slant stack.

Observing Figure 2.9, we wish to find a relation between t and f. The offset, f, at which the maximum contribution to the slant sum occurs, is equal to twice the horizontal interval Δx. Recall from the discussion of interpretation coordinates that Δx is the difference between x and x'. Review of Figure 2.13 shows that this offset is a function of reflector depth, z. We shall identify this particular offset as f_m because it represents the "middle" of a Fresnel zone.

We begin with equation (2.13) and use the claim that $f_m(z) = 2\,\Delta x(z)$. Substitution of $v\,t_0 / 2$ for z has already been done.

$$f_m(t_0) = \frac{p\,v^2\,t_0}{(1-p^2v^2)^{1/2}} \qquad \text{(A7)}$$

Now we combine equation (2.10b) with the above result to obtain

$$f_m(t) = p\,v^2\,t \qquad \text{(A8)}$$

If we draw a line from the origin of a common shot (or geophone) gather through all the points of tangency on the family of hyperbolas, we would find that equation (A8) is the equation which describes that line.

We would now like to reverse the roles of f and t in equation (A8) and assign $t_m(f)$ to be that time on a trace with offset f which is the center of a Fresnel zone for stacking parameter p. We then have

$$t_m(f) = \frac{f}{p\,v^2} \qquad \text{(A9)}$$

Figure A4 shows the interpretation of equation (A9).

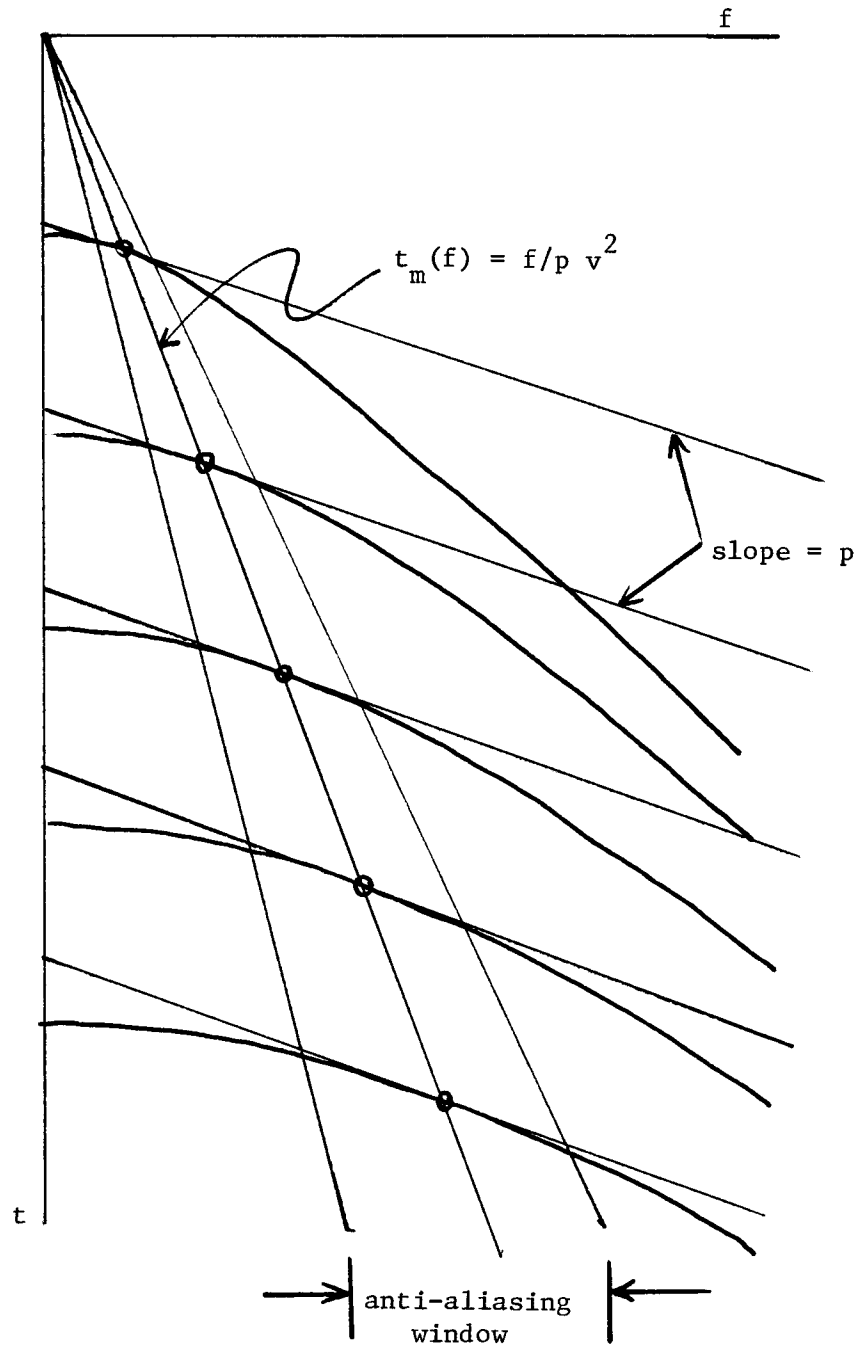

Figure A4.

The anti-aliasing window. If we include only data in the narrow range shown in the figure, the slant summation will never produce aliased energy. To have knowledge of the optimum window shape, however, requires knowledge of both velocity and structural dip as a function of time. The parameters of the window can be made to include more than the minimum data required, since we presumably have only estimates of velocity and structural dip.

A structural dip of $\pm\phi$ affects the anti-aliasing window by shifting the mean window position from θ_m to $\theta_m \pm 2\phi$. So, unknown dip can be compensated by making $\Delta\theta$ as large as possible.

We wish to include all energy into the summation which propagates within some range $\Delta\theta$ from the main angle of propagation, θ . We now define the quantities

$$t_{min}(f) = \frac{f}{p_{max}v^2} \tag{A10a}$$

and

$$t_{max}(f) = \frac{f}{p_{min}v^2} \tag{A10b}$$

Now since

$$p = \frac{\sin\theta}{v}$$

we write

$$p_{min} = \frac{\sin(\theta-\Delta\theta)}{v} \tag{A11a}$$

and

$$p_{max} = \frac{\sin(\theta+\Delta\theta)}{v} \tag{A11b}$$

or

$$p_{min} = \frac{\sin[\arcsin(pv) - \Delta\theta]}{v} \tag{A12a}$$

and

$$p_{max} = \frac{\sin[\arcsin(pv) + \Delta\theta]}{v} \tag{A12b}$$

Combining equations (A12) with (A10)

$$t_{max}^{min}(f) = \frac{f/v}{\sin(\arcsin(pv) \pm \Delta\theta)} \tag{A13}$$

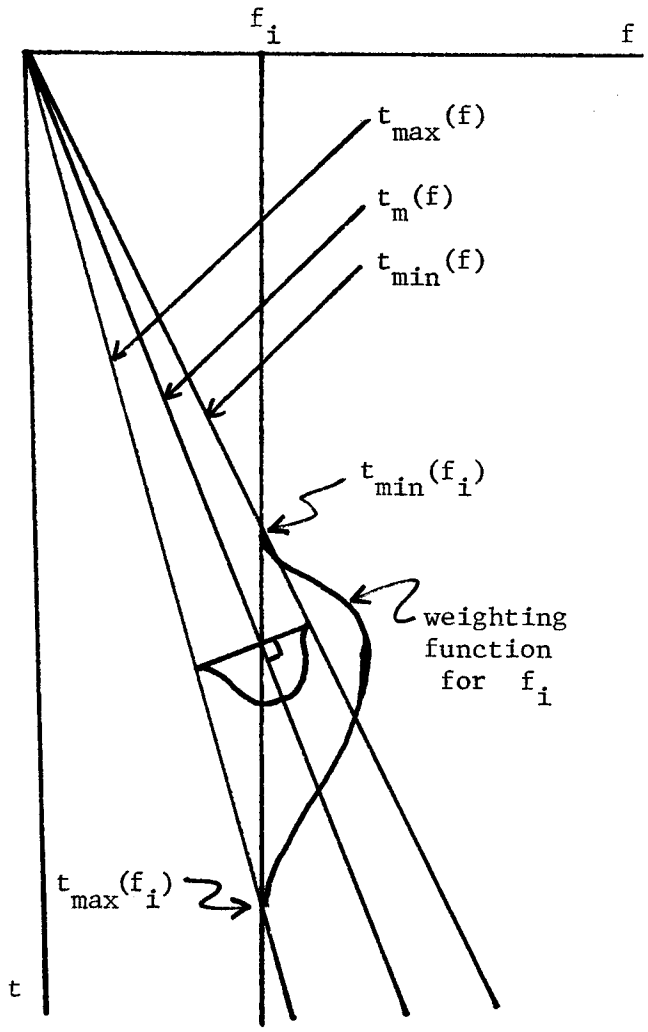

Figure A5. The anti-aliasing window of Figure A4 shown with a weighting function applied. As described in the text, we wish to design a tapering function along a perpendicular to the main radial trace. This can then be projected on to a single trace, producing a set of weights along a trace. One can show by similar triangles that for a given value of p , the weighting function for a single trace thus determined is identical to the weighting functions for all traces in the gather but with some simple scaling factors.

So, equation (A13) shows that the two quantities t_{max} and t_{min} are determined by the fixed quantity $\Delta\theta$. Setting the value of $\Delta\theta$ determines the size of the anti-aliasing window. We have determined that the Fresnel zone involves an angular window $2\,\Delta\theta = 10°$. We will always want to make this quantity somewhat larger to compensate for errors in first velocity estimate, structural dip, and energy contributing to the stack from near to, but outside the first Fresnel zone. The figures at the back of this section show slant stacks at two values of $\Delta\theta$.

Equation (A13) gives the window for a constant velocity medium. The generalization of (A13) to $v = v(z)$ is not as simple as replacing v with $v_{rms}(z)$, but a similar formula to (A13) can be derived.

The taper on the anti-aliasing window was made to be the cosine function

$$\text{taper}(\delta\theta) = \frac{1}{2}\left[\cos\left(\frac{\pi\,\delta\theta}{\Delta\theta}\right) + 1\right] \qquad \text{(A14)}$$

where $\delta\theta$ is the deviation of the propagation angle from the main angle, θ_m , which is predicted from $p = \sin\theta_m / v$.

Now, for some value of time and offset in a common shot gather,

$$\delta\theta(f,t) = \theta_m - \theta(f,t) = \sin^{-1} p\,v - \sin^{-1}\left(\frac{f}{vt}\right) \qquad \text{(A15)}$$

So, equation (A13) defines the limits of the anti-aliasing window, while (A14) and (A15) define the taper, depicted in Figure A5.

Figures A6 through A8 show slant stacks on synthetic gathers using the methods just described to reduce end effects and aliasing. Figure A6 shows the synthetic gather from which all the slant stacks

were made. All figures have the same amplitude scaling (they clip at the same amplitude) and show to what extent the slant stacked data are a partial coherency stack.

The methods described here are not intended to be the last word on the subjects of end effect and aliasing reduction. They are a first stab at these troublesome problems, and they have the advantage of being computationally cheap. (It takes less CPU time to perform a slant stack with the end effect reduction and anti-aliasing window than without them.)

Some clear deficiencies exist, however, in the realm of velocity estimation. This becomes clear from the final figures which indicate trouble when v_{stk} differs from the true velocity by more than 20%. This is hardly an adequate situation when velocity estimation is the intent. Our experience with synthetic and field data examples, however, have shown that in terms of velocity estimation, the parameters v_{stk} and $\Delta\theta$ are of less importance than they are in the visual display. We have made velocity estimations on data slant stacked with v_{stk} equal to the true velocity and also with v_{stk} 20% greater than the true velocity with no discernable differences in the output velocity profiles. In any case, it should be possible to devise a more sophisticated end effect reduction and anti-aliasing scheme which is less sensitive to the accuracy of the input velocity.

Figure A6. The common shot (or geophone) gather from which all subsequent plots of slant stacks were created, and the p-gather resulting from a simple slant stack with no provisions for end effect and aliasing reduction. Three events were generated with the same velocity of 5700 ft/sec, and a mute was introduced (shown as the diagonal straight line). These plots and those of Figures A7 and A8 all have the same amplitude scaling factor (all clip at the same amplitude) showing the extent to which the slant stack is a partial coherency stack. Waveform sizes should be compared with care since the common shot gather has a different time scale than those subsequent. The stack does indeed stretch the waveform, but apparently by only about 10%. For trace i on the common shot gather the offset, f, is $746 + 220\,i$ feet.

The p-gather shows clearly the end effects and aliasing. Compare with Figure A1. End effects are labeled on the third event, E_1E_2 for the near trace, and F_1F_2 for the far trace. Aliasing is evident in regions labeled "a". For trace i, the value of p is $i / (48 \times 5800)$. The propagation angle 30 degrees is noted on all p-gathers.

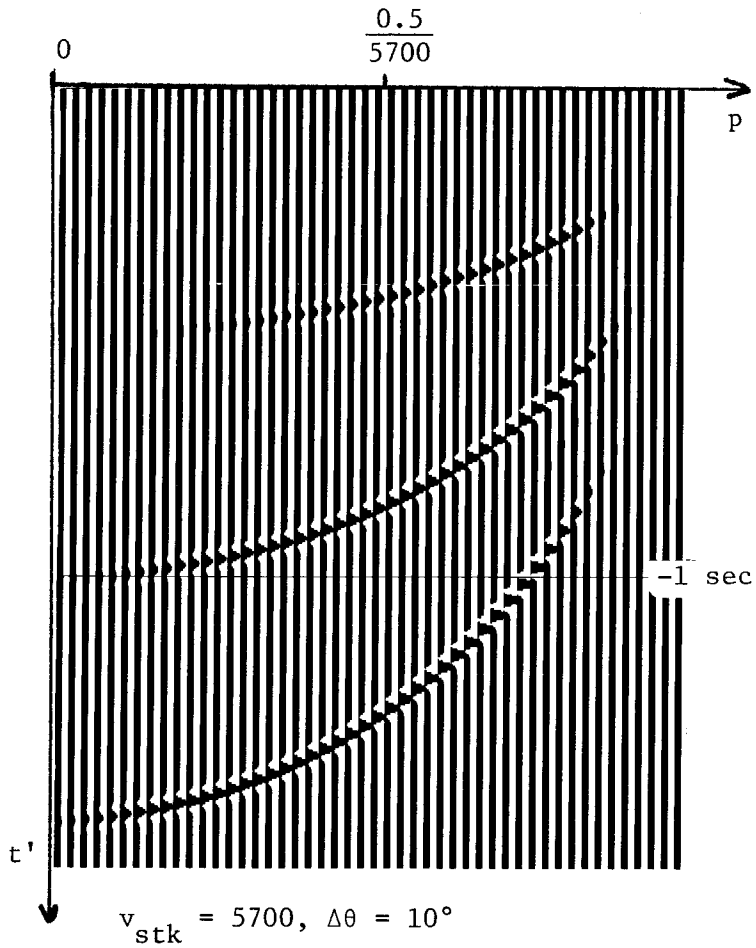

v_{stk} = 5700, $\Delta\theta$ = 10°

v_{stk} = 5700, $\Delta\theta$ = 20°

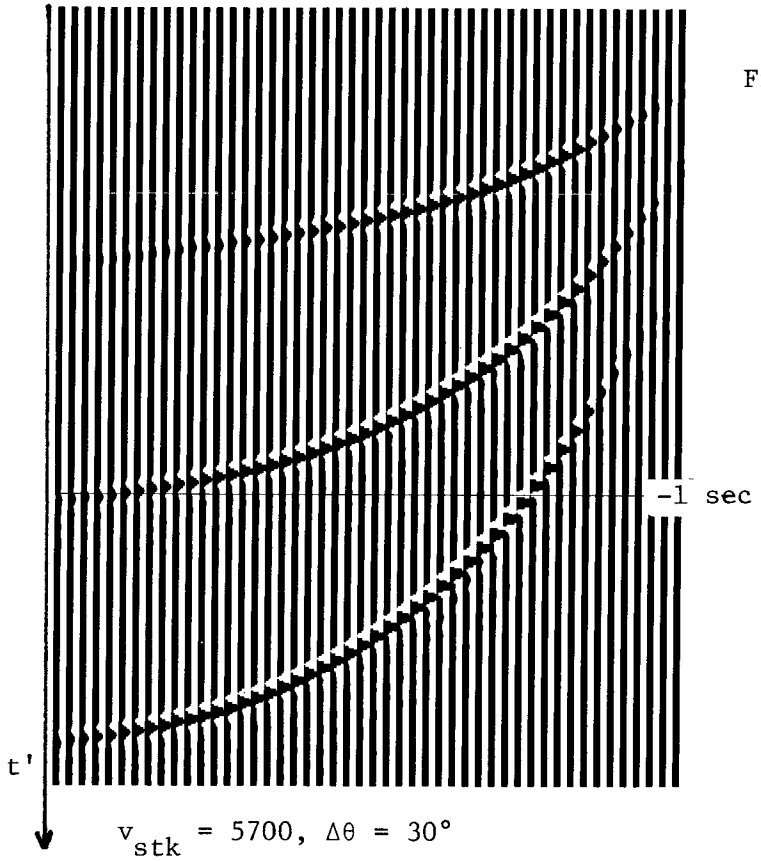

v_{stk} = 5700, $\Delta\theta$ = 30°

Figure A7. Slant stacks using the anti-aliasing window and end effect reduction scheme derived in the text. v_{stk} is the input stacking velocity and $\Delta\theta$ is the window width parameter. For all plots on this page v_{stk} is equal to the true velocity.

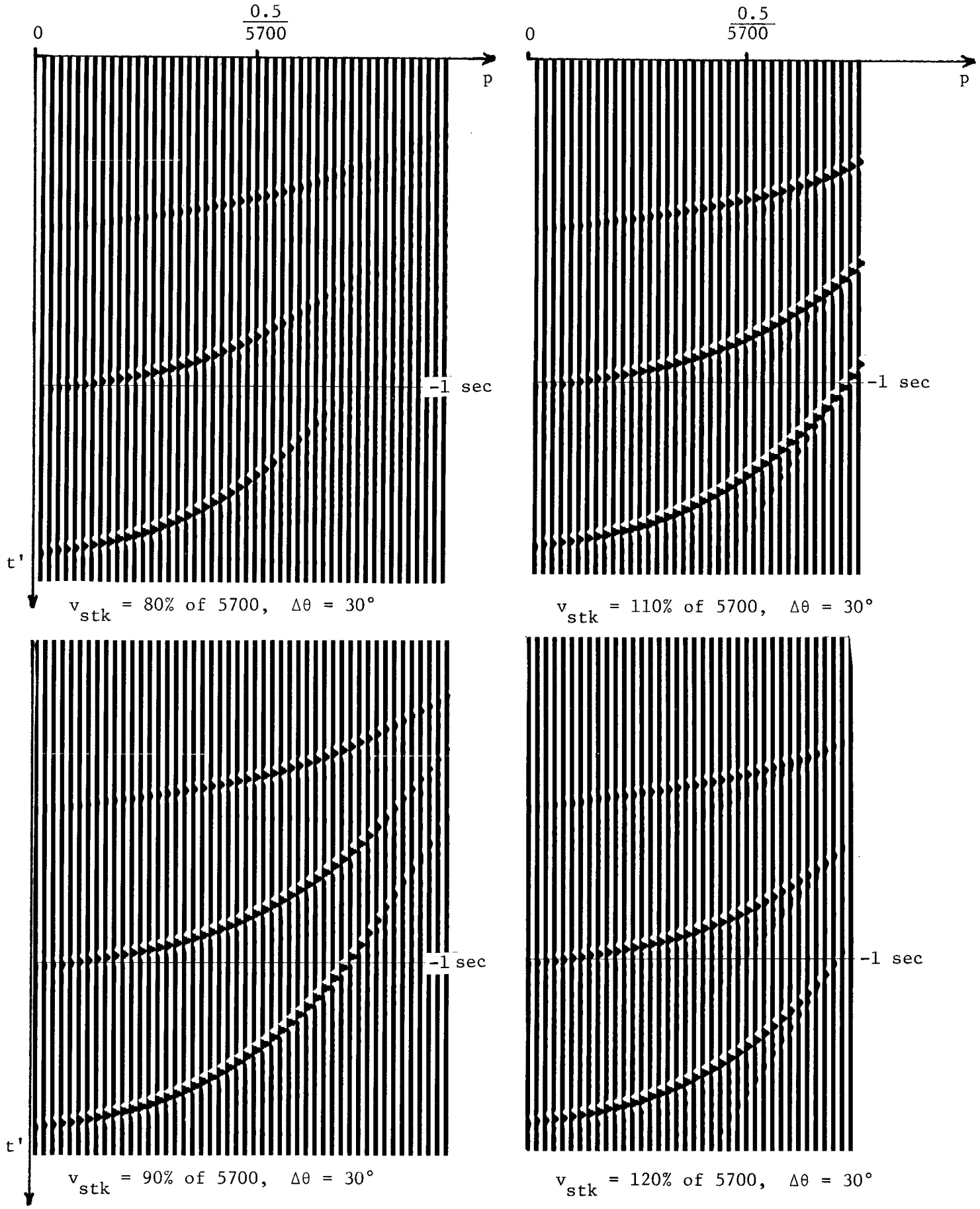

Figure A8. Slant stacks as in Figure A7, but with an incorrect stacking velocity.